

3-D Flexible Nano-Textured High-Density Microelectrode Arrays for High-Performance Neuro-Monitoring and Neuro-Stimulation

S. R. I. Gabran, *Member, IEEE*, Muhammad Tariqus Salam, *Member, IEEE*, Joshua Dian, Youssef El-Hayek, J. L. Perez Velazquez, Roman Genov, *Senior Member, IEEE*, Peter L. Carlen, M. M. A. Salama, *Fellow, IEEE*, and Raafat R. Mansour, *Fellow, IEEE*

Abstract—We introduce a new 3-D flexible microelectrode array for high performance electrographic neural signal recording and stimulation. The microelectrode architecture maximizes the number of channels on each shank and minimizes its footprint. The electrode was implemented on flexible polyimide substrate using microfabrication and thin-film processing. The electrode has a planar layout and comprises multiple shanks. Each shank is three mm in length and carries six gold pads representing the neuro-interfacing channels. The channels are used in recording important precursors with potential clinical relevance and consequent electrical stimulation to perturb the clinical condition. The polyimide structure satisfied the mechanical characteristics required for the proper electrode implantation and operation. Pad postprocessing technique was developed to improve the electrode electrical performance. The planar electrodes were used for creating 3-D “Waterloo Array” microelectrode with controlled gaps using custom designed stackers. Electrode characterization and benchmarking against commercial equivalents demonstrated the superiority of the Flex electrodes. The Flex and commercial electrodes were associated with low-power implantable responsive neuro-stimulation system. The electrodes performance in recording and stimulation application was quantified through *in vitro* and *in vivo* acute and chronic experiments on human brain slices and freely-moving rodents. The Flex electrodes exhibited remarkable drop in the electric impedance (100 times at 100 Hz), improved electrode–electrolyte interface noise (dropped by four times) and higher signal-to-noise ratio (3.3 times).

Index Terms—Flexibility, intracortical electrodes, nano-texturing, neuro-interfacing, 3-D microelectrode arrays.

Manuscript received November 02, 2013; revised March 17, 2014; accepted April 22, 2014. Date of publication May 22, 2014; date of current version September 04, 2014.

S. R. I. Gabran is with the Department of Electrical and Computer Engineering and with the Center for Integrated RF Engineering (CIRFE Lab), University of Waterloo, Waterloo, ON, N2L3G1 Canada.

M. T. Salam and R. Genov are with the Department of Electrical and Computer Engineering, University of Toronto, Toronto, ON, M5S3G4 Canada.

J. Dian, Y. El-Hayek and P. L. Carlen are with the Toronto Western Research Institute, Epilepsy Program, University Health Network, University of Toronto, Toronto, ON, M5S3G4 Canada.

J. L. Perez Velazquez is with the Neurosciences and Mental Health Research Institute, Hospital for Sick Children, Toronto, ON, M5G 1X8 Canada.

M. M. A. Salama and R. R. Mansour are with the Department of Electrical and Computer Engineering, University of Waterloo, ON, N2L 3G1 Canada.

Color versions of one or more of the figures in this paper are available online at <http://ieeexplore.ieee.org>.

Digital Object Identifier 10.1109/TNSRE.2014.2322077

I. INTRODUCTION

INTRACRANIAL recording and functional electric stimulation demonstrated promise in clinical studies and have the potential to provide treatments for neurological disorders. Recently, high-density microelectrode arrays offer new venue for investigating neural pathway and relationships between neural activities in brain and the corresponding behavior. Furthermore, functional electric stimulation (FES) may restore lost functional behavior of the damaged sensory nerves, such as auditory [1], visual [2], and somatosensory [3], Parkinson’s disease [4], and Epilepsy prostheses [5].

During the past decades, intracranial electrodes have been developed to study the functions of the nervous system. Microelectrodes were introduced in the form of glass micropipettes providing limited single-site *in vitro* recording for research applications [5]. Microwire bundle electrodes were developed to replace glass micropipettes in rodent and primate signal recordings procedures offering multiple recording sites [6]–[8]. These electrodes are limited to single channel per wire and offer lower electrode tip positional accuracy. Microelectrode arrays evolved through a number of innovations with the advancement of microfabrication technologies and fabrication techniques. Thin-film electrodes were developed on silicon wafers [9]. The use of silicon substrates for electrode fabrication was beneficial because the silicon microfabrication processes used in the microelectronics industry offer precise control of the layout and dimensions of the electrode. This process enabled the production of multichannel recording sites on a single shank without increasing the cross-sectional area.

Neuro-interfacing, neuromodulation, and investigations require electrode arrays with large number of channels capable of providing high spatial resolution recordings. Multi-shank microelectrode arrays expand the number of channels available for mapping the spatio-temporal dynamics of neuronal networks activities. Multi-shank microelectrodes developed for neural spike recording were designed to have small dimensions (surface area $\sim 150\text{--}700 \mu\text{m}^2$) in order to reduce tissue trauma [10]–[16]. However, small area yields undesirable high electrode impedance which degrades the electrode electrical performance in terms of fast consumption of implanted batteries. It also introduces high levels of thermal noise which may not contaminate the large amplitude neural spikes, but

degrades the local field potentials (LFP) recordings [17]. LFP is comprised of slow voltage waves (< 100 Hz) resulting from the neural activities and containing important precursors with potential clinical relevance [18]. The LFP can be recorded using a relatively larger electrodes surface area ($\sim 10\,000\ \mu\text{m}^2$) [17].

Traditional neurostimulation studies on humans demonstrated the efficacy of relatively high stimulation currents (up to 12 mA) for anticipating the clinical conditions [19]. Accordingly, relatively large electrode area ($12\,000\ \mu\text{m}^2$) can deliver sufficient amount of charge for disrupting an organized neural event without crossing the unsafe stimulation threshold (e.g., maximum charge density of $60\ \mu\text{C}/\text{cm}^2$ per phase) [19]–[22]. The functionality of stimulation electrodes can be improved by increasing the number of stimulation and recording channels. This improves the spatial accuracy of delivering the stimulation charges. It also allows simultaneous stimulation of several neural clusters, and enables controlling the charge distribution through current steering. However, increasing the number of large area stimulation and LFP recording channels will expand the electrode dimensions which intensifies tissue trauma and the associated foreign body response and eventually degrades the electrode operation [20].

The Chronic implantation of a rigid thin-film silicon micro-electrode arrays may cause inflammation due to micromotion and tissue damage and trauma [23]. This invokes reactive astrocytes to encapsulate the recording sites which leads to degraded electrode performance. On the other hand, polymer based flexible electrodes conform to the surrounding tissue and provide stress relieving [24]. Thus they reduce postoperative tissue damage caused by brittle equivalents and improve the electrode biocompatibility [11], [25]. In conclusion, the flexible electrodes are required for chronic implants.

In this paper, we introduce the “Flex electrode” which is a flexible multi-shank electrode designed for enhancing neuro-interfacing performance in clinical applications. The electrode has a multiple metallization layer architecture in which the routing tracks are layered underneath the large area pads. The multi-shank planar electrode is used for creating the 3-D “Waterloo Array” using custom designed stackers. We also present low cost postprocessing technique developed to improve the electric performance of the electrodes. The paper also discusses the electrode mechanical design and analysis, characterization and benchmarking, as well as *in vivo* testing results.

II. ELECTRODE DESIGN AND FABRICATION

A. High-Density Microelectrode Design

The pads and routing tracks in the conventional architectures are formed on a single metallization layer and share the available shank area. Adding more pads to a shank requires expanding its dimensions. Using narrower tracks can allow increasing the pad packing per shank; but the minimum track width is limited by the resolution of the microfabrication process. Narrow tracks also yield undesirable high electrode impedance. In conclusion, decreasing the track width offers limited improvement to the number of channels, and the maximum number of pads is therefore constrained by the shank width.

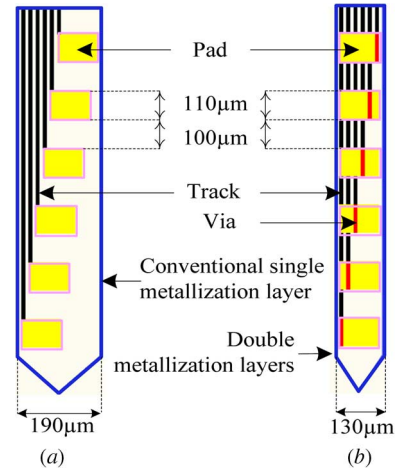


Fig. 1. Comparison of a conventional electrode (a) and the proposed double metallization layer architecture (b). Conventional design accommodates the stimulation pads (yellow) and tracks (black) on the same metal layer. Proposed architecture separates the pads and tracks into two distinct metal layers, and the associated pads and tracks are connected through buried vias (red).

The presented electrode architecture is made up of two metallization layers. The first forms the track and the second carries the exposed interconnect and stimulation pads. The metallization layers are separated by dielectric thin film, and the pads are connected to the associated routing tracks through buried vias. This architecture increases the packing of stimulation channels, and Fig. 1 compares the conventional and Flex electrode layouts and qualitatively illustrates the shank width required for packing six channels in both layouts. The proposed electrode was designed to be implemented on flexible substrates and includes an integrated interconnect cable.

The electrode is designed to be implanted in the hippocampus of small animals (rats) for neural recording and stimulation. The design requirements dictated an implantable shank length of 3 mm to reach for the targeted neural clusters, and width of $130\ \mu\text{m}$ to accommodate the required number of channels. The shank thickness was determined by the mechanical analyses (Sections II-C, II-D, and II-E) to be $100\ \mu\text{m}$. The planar electrode will be used to create 3-D array with layer gap of $150\ \mu\text{m}$.

B. Electrode Materials

Polyimide offers flexibility, chemical stability, and biocompatibility. Accordingly, it was chosen for the implementation of the structural, dielectric, and passivation layers. As for the metallization layers, gold was chosen for its biocompatibility and compatibility with the fabrication procedures used to implement the proposed designs.

C. Electrode Mechanical Design and Analysis

Flexible electrodes can be designed to provide strain relief and conform to the surrounding tissue. Therefore, they can reduce the postoperative tissue damage caused by brittle equivalents. Moreover, mechanical failure of brittle electrodes is in the form of fracture which releases debris into the tissue. Accordingly, flexible electrodes are preferred for *in vivo* and chronic applications. In order to improve the electrode biocompatibility

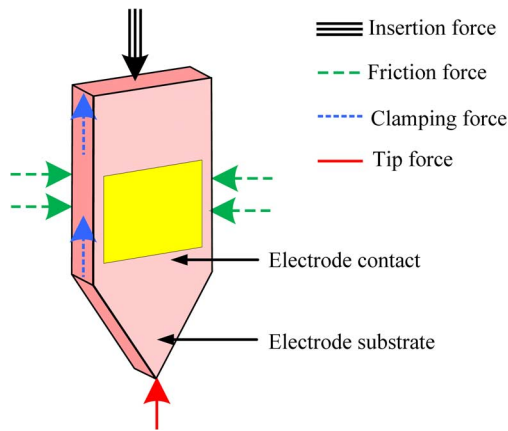


Fig. 2. Free body diagram illustrating the forces acting on the shank during insertion.

and reduce tissue trauma, it is required to minimize its footprint [26]. Reducing the electrode dimensions would compromise the rigidity required for tissue penetration. The proposed design was developed to provide lateral flexibility and axial stiffness to survive the mechanical forces experienced during insertion and operation. This design enables successful tissue penetration without the need for implantation stylus or similar stiffening devices.

The insertion force applied to the electrode must be sufficient to overcome the axial reaction forces experienced during tissue penetration. The reaction force is the superposition of the tip, clamping, and friction forces acting on the side walls and tip of the electrode, as illustrated in the free body diagram shown in Fig. 2. Based on the experimental results documented in the literature, the penetration force is estimated to be 1 mN [22], [27].

During insertion, the electrode is prone to mechanical failure and buckling [28], [29]. Ductile materials (e.g., metals and flexible polymers) respond to uniaxial stresses with elastic deformation until a yield point is reached, this is followed by plastic deformation, cracking, and fracture [30]. The proposed electrode layout was modelled and the mechanical performance was simulated using the Ansys Workbench 12 finite element modelling tool (Ansys, Canonsburg, PA, USA).

D. Buckling Analysis

Buckling is a failure mode that occurs in slender structures when the axial forces exerted on the shank exceeds a threshold value identified as the critical load and disturbs the structural equilibrium of the shank. This force drives the column into an unstable state, and the geometry of the electrode shank collapses into buckling mode. The critical instance during electrode insertion is just prior to tissue penetration, at which point the axial load and effective length of the electrode are at their maximum values [31].

To avoid buckling failure, the electrode should be designed to have a critical load beyond the force required for tissue penetration; otherwise, an insertion tool is required to support the base of the electrode while the tip propagates through the tissue. This is a fixed-pinned loading condition; however, the more stringent fixed-free configuration was assumed for safety.

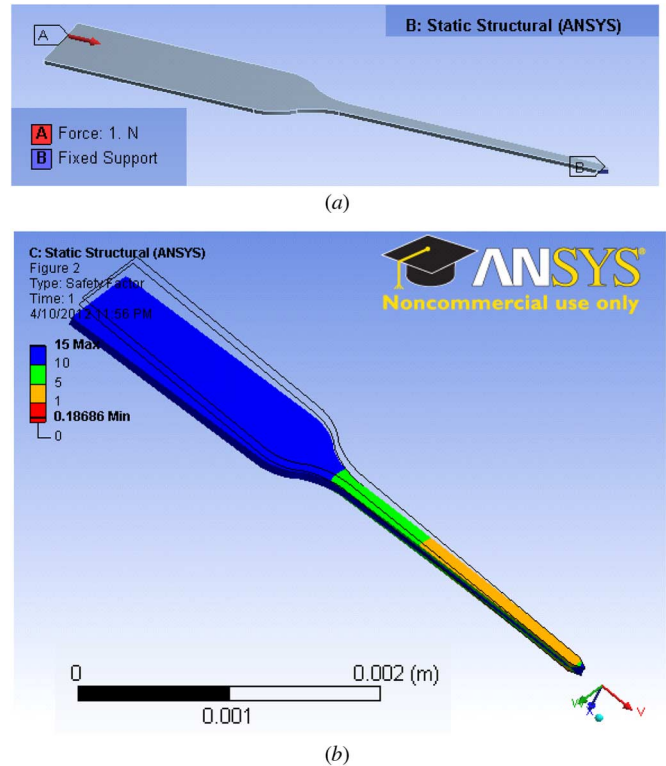


Fig. 3. (a) Fixed-free Eigen buckling model and (b) safety factor distribution for a polyimide electrode with a shank thickness of 100 μm .

The electrode was modelled for Eigen buckling analysis, and a unity axial force was applied to the electrode base (Fig. 3). A parametric model was created for design optimization, with the shank width fixed at 130 μm and the thickness was varied from 20 to 200 μm . The safety factor (SF) was calculated based on a comparison of the failure load (FL) and the design load (DL), using (1). The targeted SF value was equal to or greater than 5 [32]

$$SF = \frac{FL}{DL} = \frac{S_{Limit}}{\sigma_1} \quad (1)$$

where the failure load (S_{Limit}) is the ultimate tensile stress, or maximum shear stress, and the design load (σ_1) is the maximum tensile stress, or maximum yield strength.

E. Lateral Loading Analysis

During implantation and operation, the electrode is subjected to lateral forces normal to the shank surface which induce shear stresses [30]. The Von Mises maximum equivalent stress criterion for ductile materials was assumed to estimate electrode failures. The electrode model was configured for Von Mises stress analysis and the loading force value was set to the value of the insertion force. Fixed-free support conditions were assumed and two sets of analyses were executed. Safety factor distribution contours indicating the ratio between maximum stress and yield stress were plotted. These plots graphically illustrated the magnitude of stress levels and identified high stress regions. The provided information assisted in fine tuning the layouts to rectify regions of stress concentrations which act as stress raisers. The results showed that the minimum thickness required for the

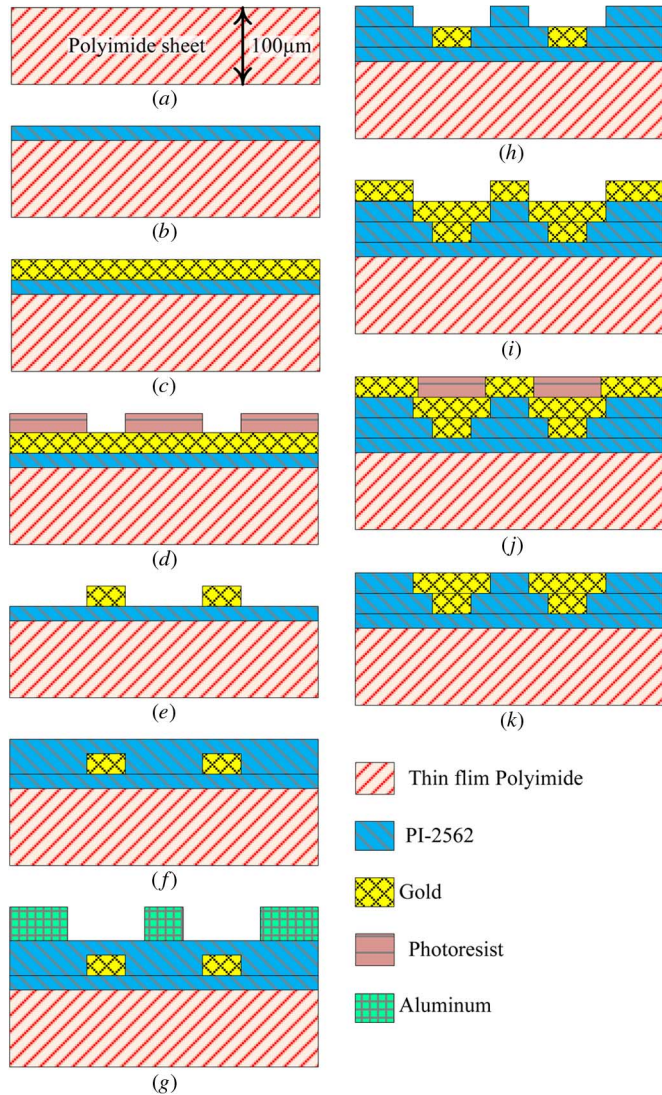


Fig. 4. Microelectrodes array fabrication steps: (a) Starting with polyimide sheet and spin coated PI-2562 and cured, (b) gold layer is deposited, (c) photoresist is patterned, then (d) gold is etched to form metallization layer-1. (e) Another polyimide layer is spin coated and cured then (f) Aluminum layer is deposited and patterned to create hardmask, then (g) polyimide is etched using oxygen plasma to create vias. (h) Gold is deposited followed by (i) applying and patterning photoresist and finally, (j) gold is etched to create metallization layer-2.

shank to survive mechanical loading was $100\ \mu\text{m}$ and the associated safety factor distribution is shown in Fig. 3(b).

F. Electrode Fabrication and 3-D Assembly

The electrode was fabricated on polyimide sheet (DuPont, USA) of thickness $100\ \mu\text{m}$ [Fig. 4(a)]. The substrate was cleaned with acetone and IPA and a thin film ($1.5\ \mu\text{m}$) of polyimide PI-2562 (HD Microsystems, USA) was spin coated (3000 RPM) and cured according to the PI-2562 standard recipe to provide a flat surface and improve adhesion to subsequent layers [Fig. 4(b)]. The first metallization layer was formed of gold (800 nm) using dc sputtering deposition and was patterned using photolithography (standard AZ-3330 recipe using Karl Suss MJB4 mask aligner) and wet etching (Transene gold etchant) to create the routing tracks [Fig. 4(c)]. The second

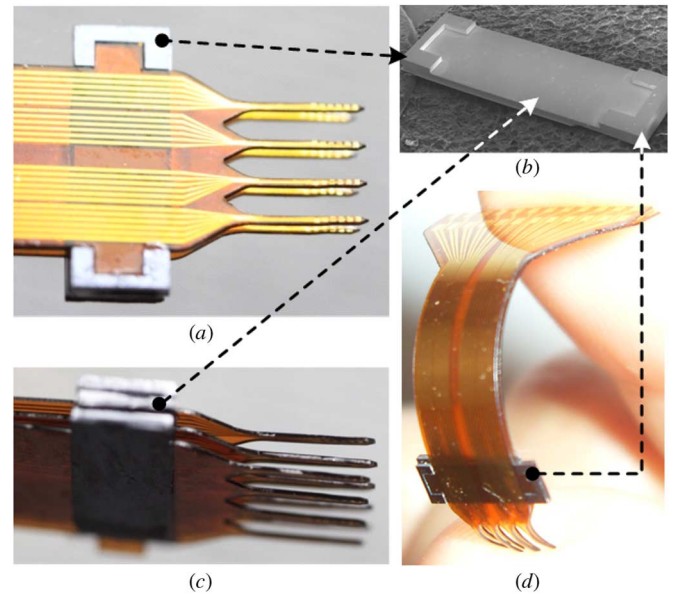


Fig. 5. Assembled Waterloo Array: (a) Planar Flex electrodes were assembled using stacking wafers, (b) SEM image of the stacking wafer, (c) side view of the Waterloo Array with 72 recording and stimulation pads, and (d) demonstrating the flexibility of the Waterloo Array.

dielectric layer (Polyimide PI-2562, HD Microsystems) was spin coated ($1.5\ \mu\text{m}$) [Fig. 4(d)] and patterned to create the buried vias using dc sputtered aluminium hard mask (400 nm) and oxygen plasma etching in Trion Technology Phantom-II Plasma Etcher RIE system [Fig. 4(e)]. The plasma etcher was set to pressure of 250 mtorr, ICP power of 100 W, RIE power of 50 W, oxygen flow of 30 sccm, and etch time of 800 s. The thin polyimide film does not interfere with the electrode mechanical performance. Finally, the second metallization layer was deposited (gold 800 nm) and patterned using photolithography and wet etching to create the exposed pads [Fig. 4(f)]. The electrode was released using laser dicing [33]. Laser dicing of the $100\ \mu\text{m}$ polyimide structures was done through professional laser dicing service provider.

An alternative release method was developed using deep reactive ion etching (DRIE). The proposed process required high-vacuum (5 mtorr), high-ICP-power (2 KW), temperature-controlled electrode ($5\ ^\circ\text{C}$) and $1\ \mu\text{m}$ aluminium mask. The process successfully etched through the $100\ \mu\text{m}$ polyimide substrate, maintaining vertical walls with undercut less than $3\ \mu\text{m}$ using Oxford Instruments PlasmaLab System 100 ICP380 DRIE etcher.

G. The Waterloo Array

The Waterloo Array is a 3-D microelectrode array formed by stacking several planar Flex electrodes [Fig. 5(a)] using custom-designed stacking wafers [Fig. 5(b)]. The implemented electrode has three layers with four shanks per layer. Each shank is 3 mm in length and carries six low impedance pads. The electrodes were aligned using the engraved aligning notches on the wafer and the projections on the electrode. The gap between the electrodes was controlled by the wafer thickness and the depth of the trench. The thickness of the wafers was $400\ \mu\text{m}$ with $250\ \mu\text{m}$ trenches and created gap of $150\ \mu\text{m}$ between the

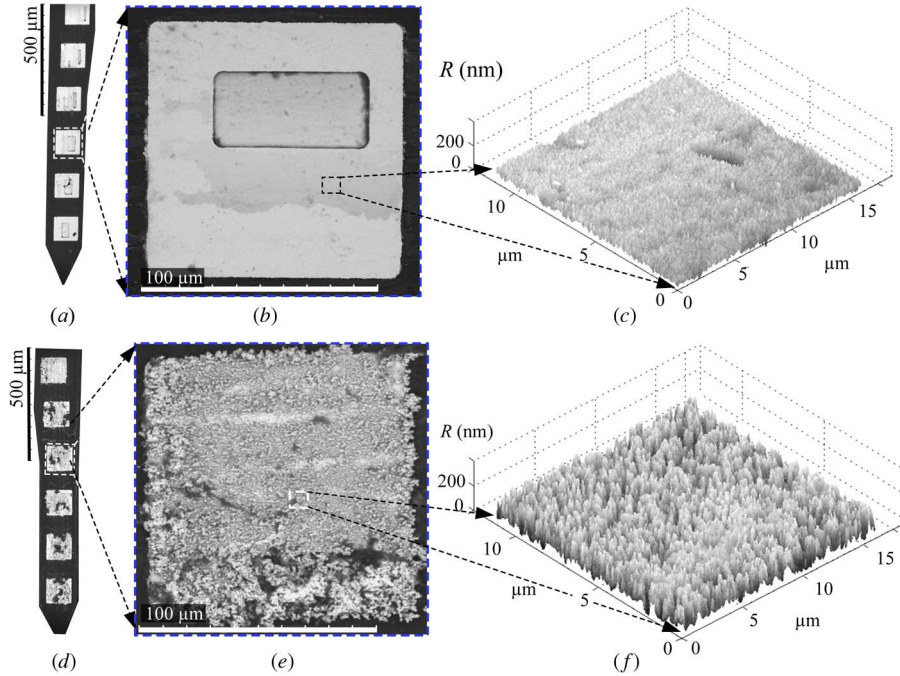


Fig. 6. Fabricated electrode pads: (a) SEM image of SME shank, (b) SEM image of a SME pad, (c) 3-D views of surface morphology SME pad, (d) SEM image of postprocessed NME shank, (e) SEM image of NME pad, and (f) 3-D views of surface morphology of NME pad.

array layers. The planar electrodes were assembled to form 3-D constellation of 72 stimulation and recording pads as shown in Fig. 5(c). Additional planar flex electrodes can be added to the assembly according to the design requirements. Fig. 5(d) illustrates the flexibility of the assembled 3-D Flex electrode array.

H. Electrode Surface Roughness

A postprocessing technique was developed in order to reduce channel impedance. The process employs low-current pulsed gold electroplating to increase the surface roughness of pad surface and expand its effective area. Fig. 6 shows the SEM pictures for the pads before (a) and after the postprocessing (d). The increase in surface roughness was inspected visually using the SEM as shown in Fig. 6(b) for the smooth surface electrode (SME) and the nanotextured microelectrode (NME) in Fig. 6(e). The increase in surface roughness was analyzed mathematically using (3).

Pad surface roughness (R) was measured using (2) and 3-D reconstructed views to illustrate the surface profiles as shown in Fig. 7(c)–(f)

$$R(i, j) = |x(i, j) - \bar{x}| \quad (2)$$

where $x(i, j)$ is the normalized individual height value of the surface and \bar{x} the mean value of all the height data points. The number of measurement points is $N \times M$, where $i = 1, 2, 3 \dots N$ and $j = 1, 2, 3 \dots M$. The root mean square (rms) roughness (R_q) is calculated from the standard deviation of the height data according to (3) [34]

$$R_q = \frac{1}{N} \left(\sum_{i=1}^N \frac{1}{M} \left(\sum_{j=1}^M (x(i, j) - \bar{x})^2 \right) \right) \quad (3)$$

R_q describes the deviation of the measurement points to the centerline and this way describes the variability of the measured profile from centerline [35].

I. Electrode Characterization

The accurate operation of the electrode and the appropriate configuration of the stimulation and recording circuits require the characterization of the electrode–tissue interface impedance. The interface impedance was measured using frequency response analysis (FRA) and electrochemical impedance spectroscopy (EIS). Two-electrode standard electrochemical cell was set up using a 0.9% sodium-chloride saline solution, platinum counter electrodes, a Solatron SI-1287 Electrochemical Interface, and a Solatron SI-1260 Impedance/Gain-Phase Analyzer. To measure the impedance, a 10 mV signal was swept from 1 MHz down to 0.1 Hz, and the current was recorded. The real and imaginary impedance components and Bode plots for the magnitude and phase were all plotted.

J. Noise Measurement

Following the impedance characterization, noises generated from the electrodes were quantified in order to calculate signal-to-noise ratio of the recorded neural signals. The electrode noise was measured using a three-step method by measuring 1) instrumentation noise, 2) reference system noise, and 3) microelectrode system noise. These measurements were done in a standard physiological saline solution using platinum reference plates (1×1 cm). First, instrument noise (V_{ni}) was measured by short circuiting the input from the amplifier. Then the reference system noise (V_{rsn}) was measured by dipping two platinum reference plates into the saline solution and

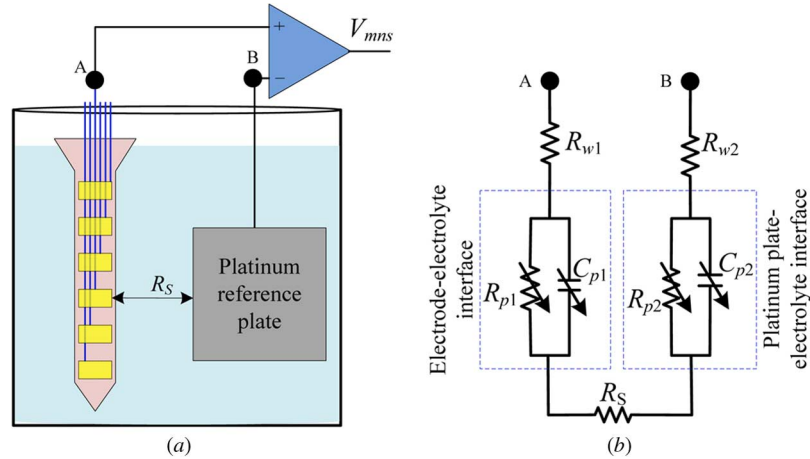


Fig. 7. Electrode noise measurement: (a) monopolar noise analysis configuration and (b) equivalent electrical circuits of platinum plate–electrolyte and electrode–electrolyte interfaces.

connecting them to the inputs of the amplifier. The measured V_{rsn} was expressed using (4).

$$V_{rsn} = V_{ni} + 2 \times V_{np} \quad (4)$$

where V_{np} is the noise generated from each platinum plate–electrolyte interface. Finally, the microelectrode system noise (V_{msn}) was similarly measured by replacing one of the platinum electrodes with the electrode under test, as illustrated in Fig. 7(a). The equivalent electrical circuit of the measurement cell is shown in Fig. 7(b), where impedance of electrode–electrolyte interface is higher than the platinum plate. The measured V_{msn} was quantified in

$$V_{msn} = V_{ni} + V_{np} + V_{nm} \quad (5)$$

where V_{nm} is the noise generated from the microelectrode–electrolyte interface. The noise signals V_{ni} , V_{np} , and V_{nm} required to estimate the signal-to-noise ratio (SNR) can be measured and calculated using this three-step noise measurement procedure.

K. In Vitro Experiment

In vitro recordings and stimulations were performed on human hippocampus brain slice (with ethic committee approval in Krembil Neuroscience Centre Research, Toronto Western Hospital, Toronto, ON, Canada). The brain slice was obtained from a resective epilepsy surgery patient and prepared for *in vitro* experiment on the same day. The brain slice was secured in place using a vacuum stage, and a stream of oxygenated (95%) artificial cerebrospinal fluid (ACSF) sustained its viability. Carbon dioxide (5%) was bubbled through the solution to buffer the bicarbonates in the ACSF. Later, the brain slice was electrically stimulated using the microelectrodes, and the stimulation pulse and evoked potentials were recorded.

L. In Vivo Experiment

The microelectrodes were validated for local field potential recordings through acute and chronic *in vivo* studies (conducted with ethic committee approval in the Neurosciences and Mental Health Research Institute, Toronto, ON, Canada). First, a Wistar rat (~250 gm) underwent craniotomy with general

anaesthesia, and the four different types of microelectrodes (commercial thin-film microelectrodes (CME) [14], and commercial microwire electrodes (CMW) [36], SME, and NME) were implanted through the somatosensory area into the hippocampus in an acute experiment. Neural signals were recorded using bipolar arrangement at 200 Hz sampling frequency (F_s) using commercial amplifier (Biopac Inc.). Later, the quality of the recorded neural signals was evaluated offline using the SNR estimation tool in MATLAB. The recorded neural signal V_{in} was divided into M segments of N sec and calculate SNR based on the following:

$$\text{SNR} = \frac{1}{M} \sum_{i=1}^M \frac{\sqrt{\sum_{k=1}^{N \times F_s} \frac{V_{in,i}(k)^2 - V_{msn,i}(k)^2}{N \times F_s}}}{\sqrt{\sum_{k=1}^{N \times F_s} \frac{V_{msn,i}(k)^2}{N \times F_s}}} \quad (6)$$

where $i = 1, 2, 3, \dots, M$, and $k = 1, 2, 3, \dots, N$. The SNR of the recording improves with the signal strength while reducing the system noise.

Following the acute experiment, another Wistar rat underwent craniotomies for chronic *in vivo* neural signal recordings. The Flex electrode [shown in Fig. 8(a) and (b)] was implanted in the rat's right hippocampus through somatosensory area [Fig. 8(c)]. On the other side, in the left hippocampus, a microwire electrode with micro-cannula was implanted for seizure inducing drug (4-aminopyridine) injection [Fig. 8(d)]. After the implantation and postoperative care, the neural signals were recorded in monopolar arrangement at 1 kHz using the flexible microelectrodes from this freely-moving animal. Also, seizures were evoked by injecting seizure induction drug and visually inspecting the high-frequency neural signal recordings using the electrodes.

III. RESULTS

Two types of Flex electrode array were assembled: type-A [Fig. 9(a)] for *in vitro* and type-B [Fig. 9(b)] for *in vivo* experiments. Both type-A and type-B arrays were bonded into a miniaturized printed circuit board (PCB). Type-A electrode was

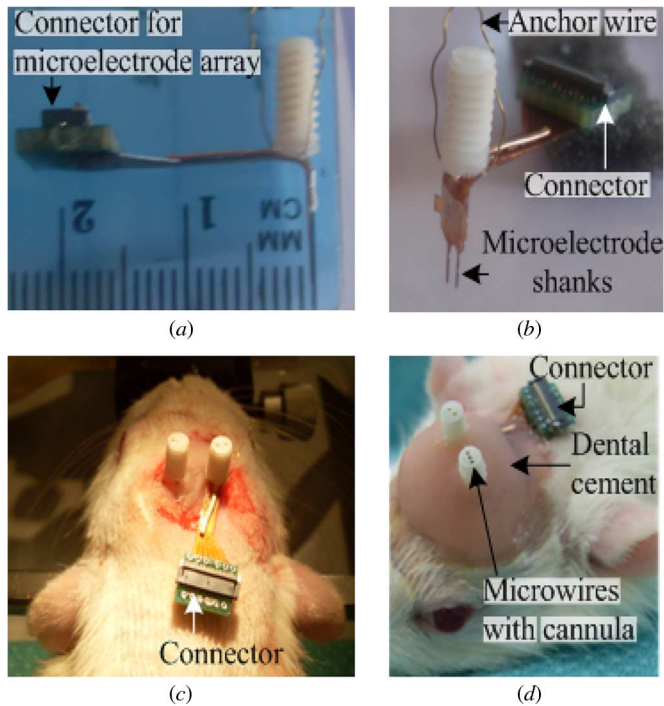


Fig. 8. Microelectrode implantation procedure in the rat brain: (a)–(b) customized flexible microelectrode array with its connector, (c) microelectrode array and micro-cannula after the implantation, (d) surgical site covered with dental cement.

attached to custom-designed PCB that provided access to the 24 channels using 1 mil pin header connectors. The dual shank type-B array was attached to another custom-designed PCB and coupled with a headset connector through a flexible wire. Summary of the comparison and benchmarking results between the Flex and commercial electrodes is listed in Table I.

A. Electrode Surface Roughness

The Flex SME had $\sim 0.12 \mu\text{m}$ rms roughness, and similarly the commercial electrodes. On the other hand, Flex NME had rms roughness of $\sim 0.56 \mu\text{m}$.

B. Electrical Impedance Spectroscopy

The impedance values of the Flex SME and NME electrodes were measured and compared to those of the commercial CME and CMW electrodes. The measured impedance values were plotted as shown in Fig. 10. Results show that the Flex NME exhibits the lowest channel impedance with an average value of $30 \text{ k}\Omega$ at 100 Hz , followed by the microwire electrode at $500 \text{ k}\Omega$, and an average value of $3 \text{ M}\Omega$ for the SME and CME. Thus, the pad postprocessing remarkably dropped the impedance by a factor of up to 100.

C. Noise Measurement

The measured input noise (V_{ni}) of the amplifier was $\sim 7 \mu\text{V}_{\text{rms}}$, and the reference system noise V_{rsn} was approximately the same value of V_{ni} because of the negligible amount of platinum plat-electrolyte interface noise contribution ($V_{ni} \gg V_{np}$) from the wider surface area in the platinum plates

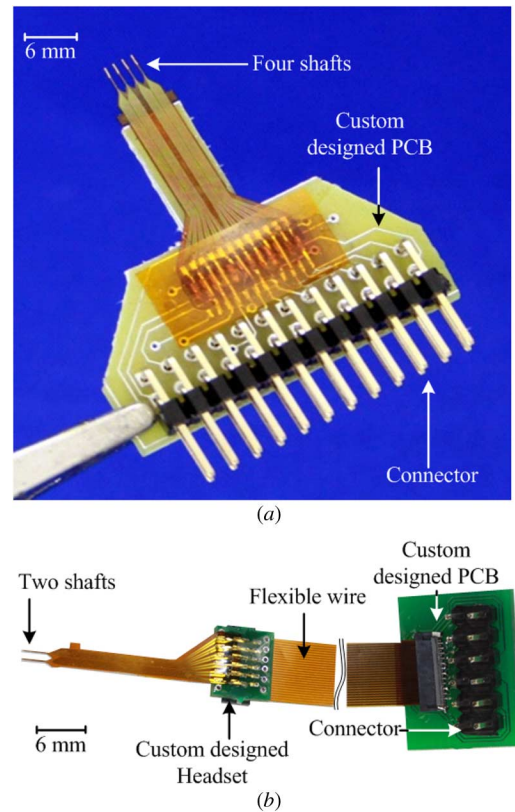


Fig. 9. Assembled microelectrode array for: (a) *in vitro* brain slice recording and stimulation, and (b) *in vivo* acute and chronic neural signal recordings.

TABLE I
COMPARISON WITH THE COMMERCIAL ELECTRODES

Characteristic	Commercial electrode		This work	
	CME [14]	CMW [36]	SME	NME
Electrode area (μm^2)	177	12000	12100	12100
Roughness (μm)	0.12	0.15	0.13	0.56
Theoretical thermal noise (μV_{rms})	7.8	3.2	7.1	0.9
Noise contribution (μV_{rms})	8.2	4.1	6.5	1.
Impedance at 100Hz (Ω)	3 M	500 k	3 M	30 k
Signal to noise ratio	2.2	5.3	4.1	12.4

[37]. Fig. 11 depicts the flicker noise domination in the V_{ni} at a lower frequency band (below 3 Hz); however, the thermal noise of amplifier is spectrally flat or has a uniform noise density over the wide frequency band. On the other hand, the microelectrode system noise V_{msn} is higher at lower frequencies due to the amplifier's flicker noise and the uniformly distributed thermal noises of the electrode impedance and amplifier over the wide frequency band. The lowest microelectrode system noise was generated by the Flex NME which was about four times lower at 70 Hz compared to the commercial CME or CWE. The electrode thermal rms noise is directly proportional to its resistive properties. The smaller contacts in the commercial electrodes introduced higher impedance as shown in Fig. 10, and consequently higher thermal rms noise, as shown in Fig. 11. This would degrade the SNR values of the LFP recordings; nevertheless, it will not affect the high amplitude neural spikes.

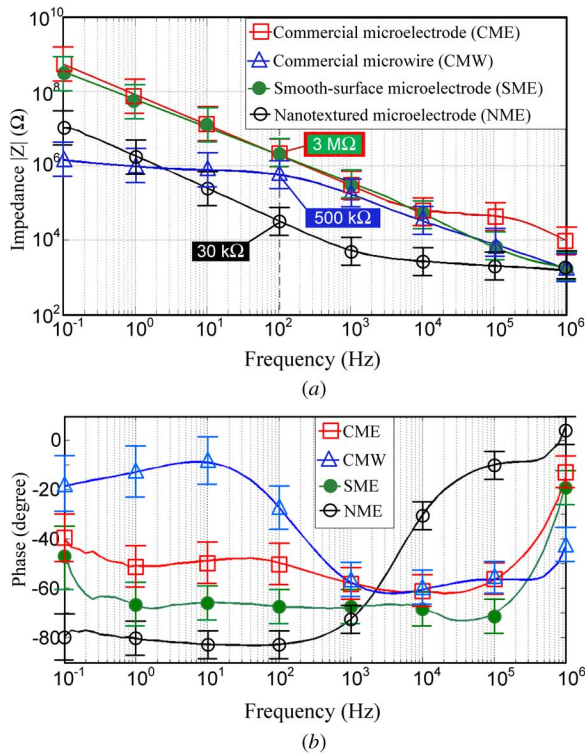


Fig. 10. Impedance characterization results using EIS: (a) impedance and (b) phase curves.

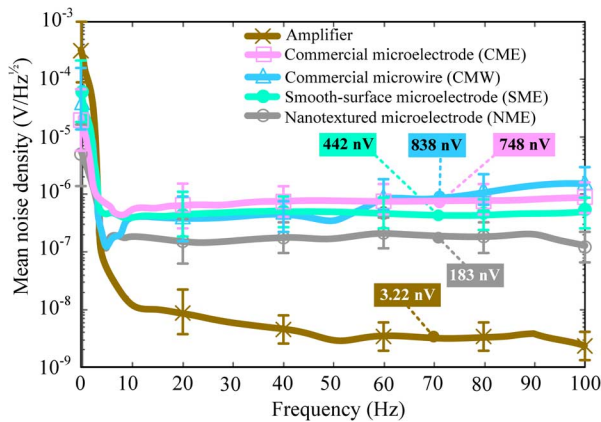


Fig. 11. Measured instrumentation noise and microelectrode system noise densities.

However, the NME exhibited the lowest impedance characteristic compared to other microelectrodes as demonstrated in Fig. 10. This is due to the larger electrode area and increased surface roughness. As a result, the NME’s system rms noise within 3–100 Hz (the LFP recording band) is approximately four times lower compared to other electrodes.

D. In Vitro Experiment

Neuro-stimulation was performed *in vitro* human brain slice using the Flex microelectrode. A stimulation current pulse (0.1 mA) was generated using voltage-controlled current stimulator and delivered through the microelectrodes into the brain slice. The stimulation pulse and evoked potentials were detected

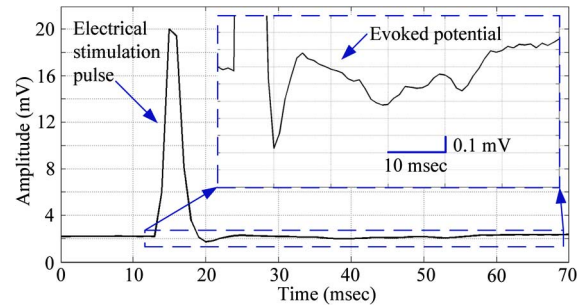


Fig. 12. Electrical stimulation *in vitro* experiment: stimulation pulse and zoom-inset shows resultant evoked potential.

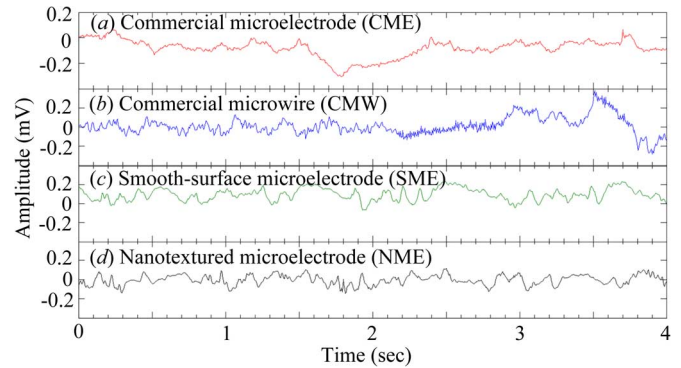


Fig. 13. *In vivo* acute neural signal recordings in rat’s hippocampus using: (a) CME, (b) CMW, (c) SME, and (d) NME.

using standard recording electrodes and captured using Peak Lab high-gain amplifier (AD Instruments Inc.). Stimulation and recording were repeated and the captured signals exhibited consistency. The recorded signals were plotted in Fig. 12 which shows the stimulation pulse followed by the evoked potential as a response to the stimulation of the hippocampus concluding the successful operation of the Flex electrode.

E. In Vivo Experiments

Fig. 13 shows samples with duration of 4 s for acute *in vivo* neural signal recordings using Flex SME and NME and commercial CME and CMW. Recording neural activities using the CME, CMW and NME suffered attenuation at the low frequencies; while CMW brought higher frequency noises. The mean spectral densities and SNR of the recordings were quantified from 280 segments of the 4 s recordings. Fig. 14 illustrates the average spectral densities of the CME, CMW, SME, and NME recordings along with their respective electrode noise levels. The CMW exhibits higher levels of electrode noise at higher frequencies, whereas the NME reveals the lowest electrode noise and yields the best overall signal fidelity with an SNR value of 18, followed by 16.1 for the SME, while the CMW achieved a value of 7.3 and 2.2 for the CME.

Fig. 15 shows 12 channels *in vivo* chronic recordings using the dual-shank Flex electrode eight weeks after implantation. These recordings show LFP and relatively higher frequencies epileptic electrographic discharges due to the seizure induction drug injection. Average SNR of the recordings is 17.6.

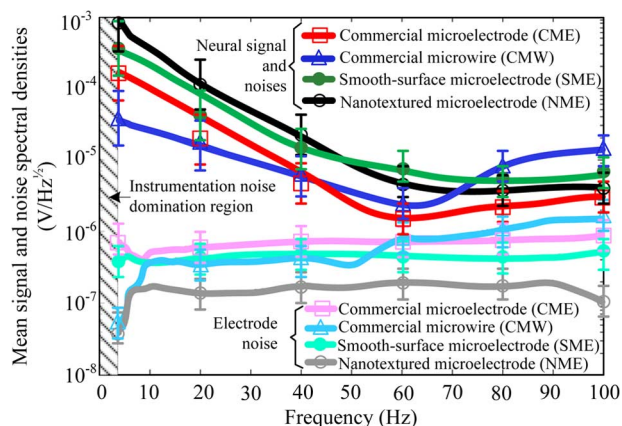


Fig. 14. Mean spectral densities of *in vivo* acute neural signal recordings and electrodes noises of: (a) CME, (b) CMW, (c) SME, and (d) NME.

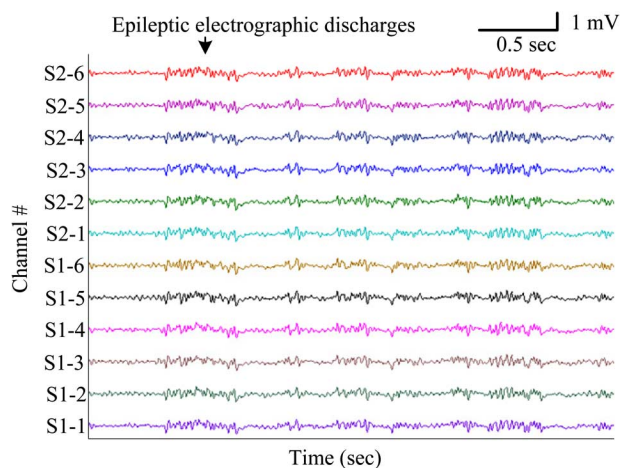


Fig. 15. *In vivo* chronic neural signal recordings from rat hippocampus using the 12 channels dual-shank flexible microelectrode array, where S1-1 is shank number 1 and electrode number 1 located at tip of the shank.

Therefore, long-term recordings using Flex electrodes are stable without a significant decrement in signal quality.

IV. CONCLUSION

In this paper, we presented new electrode architecture developed to increase the number of stimulation pads on thin film electrodes while minimizing the electrode dimensions and footprint. The electrode architecture has two metallization layers: one for the pads and the other for the routing tracks separated by a dielectric layer. The pads are connected to the associated tracks through buried vias so that the width of the shank can accommodate the pads without the dimensional overhead required for the tracks. The electrode was designed to be implemented on flexible polyimide substrates to improve its biocompatibility through reducing tissue damage and trauma. The electrode mechanical performance was simulated using finite element modelling. A low-cost postprocessing technique was developed to improve the electrode electrical performance. The planar Flex electrodes were assembled using stacking wafers to create the flexible 3-D “Waterloo Array.” The electrodes were characterized and the electrode–tissue interface impedances were measured. The electrodes were tested for *in vitro* stimulation, and

an evoked potential was successfully recorded. The electrodes were also tested through acute and chronic *in vivo* recordings, and the results were compared with those obtained with commercial electrodes. The outcome of the testing demonstrates the outstanding electrical performance of the Flex electrodes with postprocessed nano-textured surface.

ACKNOWLEDGMENT

The infrastructure used for this work would not have been possible without the significant contributions of the Natural Sciences and Engineering Research Council of Canada (NSERC), the Canada Foundation for Innovation (CFI), Canadian Microelectronics Corporation (CMC), and Ontario Brain Institute (OBI).

REFERENCES

- [1] S. Fredelake and V. Hohmann, “Factors affecting predicted speech intelligibility with cochlear implants in an auditory model for electrical stimulation,” *Hearing Res.*, vol. 287, no. 1–2, pp. 76–90, May 2012.
- [2] R. Cicione, M. N. Shivdasani, J. B. Fallon, C. D. Luu, P. J. Allen, G. D. Rathbone, R. K. Shepherd, and C. E. Williams, “Visual cortex responses to suprachoroidal electrical stimulation of the retina: Effects of electrode return configuration,” *J. Neural Eng.*, vol. 9, no. 3, p. 036009, 2012.
- [3] C. C. Kerr, S. A. Neymotin, G. L. Chadderdon, C. T. Fietkiewicz, J. T. Francis, and W. W. Lytton, “Electrostimulation as a prosthesis for repair of information flow in a computer model of neocortex,” *IEEE Trans. Neural Syst. Rehabil. Eng.*, vol. 20, no. 2, pp. 153–160, Mar. 2012.
- [4] C. Seifried, L. Weise, R. Hartmann, T. Gasser, S. Baudrexel, A. Szelényi, S. van de Loo, H. Steinmetz, V. Seifert, J. Roepfer, and R. Hilker, “Intraoperative microelectrode recording for the delineation of subthalamic nucleus topography in Parkinson’s disease,” *Brain Stimulat., Basic, Translat., Clin. Res. Neuromodulat.*, vol. 5, no. 3, pp. 378–387, Jul. 2012.
- [5] D. J. DiLorenzo and J. D. Bronzino, *Neuroengineering*. Boca Raton, FL: CRC Press, 2007.
- [6] K. Kagoo, *Microelectrode Arrays for Neural Recording*. School of Engineering, UCSC, 2005.
- [7] J. Ji and K. D. Wise, “Scaling limitations of silicon multichannel recording probes,” *IEEE Trans. Biomed. Eng.*, vol. 37, no. 1, pp. 1–11, Jan. 1990.
- [8] W. He and R. V. Bellamkonda, “A molecular perspective on understanding and modulating the performance of chronic Central Nervous System (CNS) recording electrodes,” in *Source Indwelling Neural Implants: Strategies for Contending With the In Vivo Environment*, W. M. Reichert, Ed. Boca Raton, FL: CRC Press, 2008, ch. 6.
- [9] K. D. Wise, J. B. Angell, and A. Starr, “An integrated-circuit approach to extracellular microelectrodes,” *IEEE Trans. Biomed. Eng.*, vol. 17, no. 3, pp. 238–247, Jul. 1970.
- [10] R. Biran, D. C. Martin, and P. A. Tresco, “The brain tissue response to implanted silicon microelectrode arrays is increased when the device is tethered to the skull,” *J. Biomed. Mater. Res. A*, vol. 82, no. 1, pp. 169–178, 2007.
- [11] K. C. Cheung, P. Renaud, H. Tanila, and K. Djupsund, “Flexible polyimide microelectrode array for *in vivo* recordings and current source density analysis,” *Biosens. Bioelectron.*, vol. 22, pp. 1783–1790, 2007.
- [12] Y. Y. Chen, H. Y. Lai, S. H. Lin, C. W. Cho, W. H. Chao, C. H. Liao, S. Tsang, Y. F. Chen, and S. Y. Lin, “Design and fabrication of a polyimide-based microelectrode array: Application in neural recording and repeatable electrolytic lesion in rat brain,” *J. Neurosci. Methods*, vol. 182, no. 1, pp. 6–16, 2009.
- [13] F. Shahrokhii, K. Abdelhalim, D. Serletis, P. Carlen, and R. Genov, “128-channel fully differential digital integrated neural recording and stimulation interface,” *IEEE Trans. Biomed. Circuits Syst.*, vol. 4, no. 3, pp. 149–161, Jun. 2010.
- [14] NeuroNexus: Electrode arrays Accessed on March 8, 2013 [Online]. Available: <http://www.neuronexustech.com>
- [15] G. Schneider and D. Nikolić, “Detection and assessment of near-zero delays in neuronal spiking activity,” *J. Neurosci. Methods*, vol. 152, no. 1–2, pp. 97–106, 2006.

- [16] T. J. Blanche, M. A. Spacek, J. F. Hetke, and N. V. Swindale, "Polymers: High-density silicon electrode arrays for large-scale multiunit recording," *J. Neurophysiol.*, vol. 93, no. 5, pp. 2987–3000, 2005.
- [17] D. Xing, C. Yeh, and R. M. Shapley, "Spatial spread of the local field potential and its laminar variation in visual cortex," *J. Neurosci.*, vol. 29, no. 37, pp. 11540–11549, 2009.
- [18] J. L. Perez Velazquez, L. G. Dominguez, V. Nenadovic, and R. A. Wennberg, "Experimental observation of increased fluctuations in an order parameter before epochs of extended brain synchronization," *J. Biol. Phys.*, vol. 37, pp. 141–152, 2011.
- [19] M. J. Morrell, "Responsive cortical stimulation for the treatment of medically intractable partial epilepsy," *Neurology*, vol. 77, no. 13, pp. 1295–1304, 2011.
- [20] A. K. Koivuniemi, S. J. Wilks, A. J. Woolley, and K. J. Otto, "Multimodal, longitudinal assessment of intracortical microstimulation," *Progr. Brain Res.*, vol. 194, pp. 131–144, 2011.
- [21] B. Gordon, R. P. Lesser, N. E. Rance, J. Hart, R. Webber, S. Uematsu, and R. S. Fisher, "Parameters for direct cortical electrical stimulation in the human: Histopathologic confirmation," *Electroencephal. Clin. Neurophysiol.*, vol. 75, no. 5, pp. 371–377, 1990.
- [22] S. F. Cogan, "Neural stimulation and recording electrodes," *Annu. Rev. Biomed. Eng.*, vol. 10, pp. 275–309, 2008.
- [23] S. R. I. Gabran, M. T. Salam, J. Dian, Y. El-Hayek, J. L. Perez Velazquez, R. Genov, P. L. Carlen, M. M. A. Salama, and R. R. Mansour, "Intracortical microelectrode arrays with multiple metallization layers for high-density neuromonitoring and neurostimulation," *IEEE Trans. Neural Syst. Rehabil. Eng.*, vol. 21, no. 6, pp. 869–879, Nov. 2013.
- [24] J. Subbaroyan, D. C. Martin, and D. R. Kipke, "A finite-element model of the mechanical effects of implantable microelectrodes in the cerebral cortex," *J. Neural Eng.*, vol. 2, no. 4, pp. 103–113, 2005, [FEM].
- [25] R. R. Richardson, J. A. Miller, and W. M. Reichert, "Polyimides as biomaterials: Preliminary biocompatibility testing," *Biomaterials*, vol. 14, no. 8, pp. 627–635, 1993, [BIO].
- [26] P. K. Campbell, K. F. Jones, R. J. Huber, K. W. Horch, and R. A. Normann, "A silicon-based, three-dimensional neural interface," *IEEE Trans. Biomed. Eng.*, vol. 38, no. 8, pp. 758–768, Aug. 1991.
- [27] T. Suzuki, K. Mabuchi, and S. Takeuchi, "A 3-D flexible parylene probe array for multichannel neural recording," in *Proc. 1st Int. IEEE EMBS Conf. Neural Eng.*, 2003, pp. 154–156.
- [28] J. M. Gere and S. P. Timoshenko, *Mechanics of Materials*. Kingston, U.K.: Stanley Thornes, 1999.
- [29] T. Yi, L. Li, and C. J. Kim, "Microscale material testing of single crystalline silicon," *Sensors Actuators*, vol. 83, no. 1–3, pp. 172–178, 2000.
- [30] S. D. Senturia, *Microsystem Design*. New York: Kluwer Academic, 2002.
- [31] H. Kim and J. S. Colton, "Fabrication and analysis of plastic hypodermic needles," *J. Med. Eng. Technol.*, vol. 29, 2005.
- [32] M. Salcman and M. Bak, "Design, fabrication, and *in vivo* behavior of chronic recording intracortical microelectrodes," *IEEE Trans. Biomed. Eng.*, vol. 20, no. 4, pp. 253–260, Jul. 1973.
- [33] S. R. I. Gabran, R. R. Mansour, and M. M. A. Salama, "Maskless pattern transfer using 355 nm laser," *J. Opt. Lasers Eng.*, vol. 50, no. 5, pp. 710–716, 2012.
- [34] *Surface Texture*, ASME B-46.1-1995, 1995.
- [35] F. Podczeczek, *Factors Influencing Adhesion*. In *Book: Particle-Particle Adhesion in Pharmaceutical Powder Handling*. London, U.K.: Imperial College Press, 1997.
- [36] PlasticsOne: Multi-Channel Electrode Accessed on March 8, 2013 [Online]. Available: <http://www.plastics1.com>
- [37] A. Hassibi, R. Navid, R. W. Dutton, and T. H. Lee, "Comprehensive study of noise processes in electrode electrolyte interfaces," *J. Appl. Phys.*, vol. 96, no. 2, 2004.



S. R. I. Gabran (M'98) received the B.Sc. degree in electrical engineering from Cairo University, Cairo, Egypt, in 2002, and the M.A.Sc. and Ph.D. degrees in electrical engineering from the University of Waterloo, Waterloo, ON, Canada, in 2006 and 2012, respectively.

Currently, he is the co-founder and Director of Novela Inc. He is a Researcher with the CIRFE Lab, University of Waterloo, and NSERC industrial postdoctoral fellow. He works in collaboration with the Intelligent Sensory Microsystems Laboratory

(University of Toronto), the Krembil Neuroscience Institute and the Sick Kids Hospital. His research interests include nano-fabrication, micro-fabrication, flexible substrates, BioMEMS, neuro-engineering, intra-cortical implants, and embedded systems.

Dr. Gabran received the MEMSCAP best microsystem design award in 2013.



Muhammad Tariq Salam (M) received the B.A.Sc. degree in electrical and electronics engineering from the Islamic University of Technology, Gazipur, Bangladesh, in 2003, the M.A.Sc. degree in electrical and computer engineering from Concordia University, Montréal, QC, Canada, in 2007, and the Ph.D. degree in electrical engineering from Polytechnique Montréal, Montréal, QC, Canada, in 2012.

Currently, he is a Postdoctoral Fellow in University of Toronto where he works at Intelligent Sensory Microsystems Laboratory, Neurosciences and Mental Health institute of Hospital for Sick Children Hospital, and Neuroscience division of Toronto Western Hospital. His specific research interests are in the areas of biosensing, detection and stimulation microsystems; implantable biomedical microdevices for continuous health monitoring, cognitive brain research, mental disease diagnosis, treatment, and rehabilitations.



Joshua Dian received the B.A.Sc. degree in engineering science specializing in biomedical engineering and subsequently the M.A.Sc. degree in electrical engineering from the University of Toronto, Toronto, ON, Canada. He is currently working toward the Ph.D. degree in electrical engineering focusing the characterization and control of epileptic seizures *in vitro*.



Youssef El-Hayek received the Ph.D. degree from the Department of Physiology at the University of Toronto, Toronto, ON, Canada. Following that, he completed a postdoctoral fellowship with Dr. P. Carlen at the University Health Network, Toronto, ON, Canada. During his time there, he investigated the neurophysiology of epilepsy, aging, stroke, and Alzheimer's disease.

Dr. El-Hayek is a recipient of the Alzheimer's Society of Canada Doctoral Training award and the Canadian Institutes of Health Research "Science to

Business" award.



J. L. Perez Velazquez was born in Zaragoza, Spain. He received the degree of "Licenciado" in chemistry (biochemistry, Universities of Zaragoza and Complutense, Madrid, Spain), and the Ph.D. degree from the Department of Molecular Physiology and Biophysics, Baylor College of Medicine, Houston, TX, USA, in 1992, homologated to Doctorate in Chemistry by the Spanish Ministry of Culture in 1997.

He is an Associate Scientist in the Neuroscience and Mental Programme and the Brain and Behaviour Center at the Hospital For Sick Children in Toronto, and Associate Professor at the University of Toronto, Toronto, ON, Canada.



Roman Genov (S'96–M'02–SM'11) received the B.S. degree in electrical engineering from Rochester Institute of Technology, Rochester, NY, USA, in 1996, and the M.S.E. and Ph.D. degrees in electrical and computer engineering from The Johns Hopkins University, Baltimore, MD, USA, in 1998 and 2002, respectively.

He has held engineering positions at Atmel Corporation, Columbia, MD, USA, in 1995, and Xerox Corporation, Rochester, NY, USA, in 1996. He was a visiting researcher in the Laboratory of Intelligent Systems at Swiss Federal Institute of Technology (EPFL), Lausanne, Switzerland, in 1998, and in the Center for Biological and Computational Learning at Massachusetts Institute of Technology, Cambridge, MA, USA, in 1999. He is presently an Associate Professor in the Department of Electrical and Computer Engineering at the University of Toronto, Toronto, ON, Canada. His research interests are primarily in analog integrated circuits and systems for energy-constrained biological, medical, and consumer sensory applications, such as implantable, wearable or disposable sensory microsystems, energy-efficient sensory signal processors and wireless sensors, including brain–chip interfaces, neuro-stimulators, image sensors, optical and electro-chemical DNA microarrays, and other biosensors.

Dr. Genov is a co-recipient of Best Paper Award of IEEE Biomedical Circuits and Systems Conference, Best Student Paper Award of IEEE International Symposium on Circuits and Systems, Best Paper Award of IEEE Circuits and Systems Society Sensory Systems Technical Committee, Brian L. Barge Award for Excellence in Microsystems Integration, MEMSCAP Microsystems Design Award, DALSA Corporation Award for Excellence in Microsystems Innovation, and Canadian Institutes of Health Research Next Generation Award. He was a Technical Program co-Chair at IEEE Biomedical Circuits and Systems Conference. He was an Associate Editor of IEEE TRANSACTIONS ON CIRCUITS AND SYSTEMS—II: EXPRESS BRIEFS and IEEE SIGNAL PROCESSING LETTERS. Currently he is an Associate Editor of IEEE TRANSACTIONS ON BIOMEDICAL CIRCUITS AND SYSTEMS and member of IEEE International Solid-State Circuits Conference International Program Committee serving on Imagers, MEMS, Medical, and Displays (IMMD) Subcommittee. He was an Associate Editor of IEEE TRANSACTIONS ON CIRCUITS AND SYSTEMS—II: EXPRESS BRIEFS and IEEE SIGNAL PROCESSING LETTERS. Currently he is an Associate Editor of IEEE TRANSACTIONS ON BIOMEDICAL CIRCUITS AND SYSTEMS and serves on the Imagers, MEMS, Medical, and Displays Subcommittee of the *International Solid-State Circuits Conference*.



Peter L. Carlen is a Professor of Medicine (Neurology), Physiology, and Institute of Biomaterials and Biomedical Engineering at the University of Toronto, Toronto, ON, Canada. He is a clinician/scientist, specializing in epilepsy and neurodegenerative diseases at the Toronto Western Hospital of the University Health Network. He was formerly the Head of Neurology at the Addiction Research Foundation. In 1989, he was appointed Director of the Playfair Neuroscience Unit and Neuroscience Research at the University Health Network for a 10 year term,

where he is now a Senior Scientist and Head of the Division of Fundamental Neuroscience. He has over 250 peer-reviewed biomedical publications and six patents. His main research interests are mechanisms of neural synchrony and entrainment in the context of epilepsy, the fetal alcohol syndrome, hypoglycemic seizures, and neurodegenerative processes. He also is an active neurological clinician with a practice focused on patients with epilepsy.



M. M. A. Salama (F'02) received the B.Sc. and M.Sc. degrees in electrical engineering from Cairo University, Cairo, Egypt, in 1971 and 1973, respectively, and the Ph.D. degree in electrical engineering from the University of Waterloo, Waterloo, ON, Canada, in 1977.

Currently, he is a Professor in the Department of Electrical and Computer Engineering, University of Waterloo, Waterloo, ON, Canada. His interests include the operation and control of distribution systems, power-quality monitoring and mitigation, asset management, and electromagnetics. He has consulted widely with government agencies and the electrical industry.

Dr. Salama is a registered Professional Engineer in the Province of Ontario.



Raafat R. Mansour (S'84–M'86–SM'90–F'01) was born in Cairo, Egypt, on March 31, 1955. He received the B.Sc. (with honors) and M.Sc. degrees from Ain Shams University, Cairo, Egypt, in 1977 and 1981, respectively, and the Ph.D. degree from the University of Waterloo, Waterloo, ON, Canada, in 1986, all in electrical engineering.

In 1981, he was a Research Fellow with the Laboratoire d'Electromagnetisme, Institut National Polytechnique, Grenoble, France. From 1983 to 1986 he was a Research and Teaching Assistant with the Department of Electrical Engineering, University of Waterloo. In 1986, he joined COM DEV Ltd., Cambridge, ON, Canada, where he held several technical and management positions with the Corporate Research and Development Department. In 1998, he received the title of a Scientist. In January 2000, he joined the University of Waterloo, as a Professor with the Electrical and Computer Engineering Department. He holds a Natural Sciences and Engineering Research Council of Canada (NSERC) Industrial Research Chair in RF engineering with the University of Waterloo. He is the Founding Director of the Center for Integrated RF Engineering (CIRFE), University of Waterloo. He has authored or coauthored numerous publications in the areas of filters and multiplexers, high-temperature superconductivity and microelectromechanical systems (MEMS). He is a coauthor of *Microwave Filters for Communication Systems* (Wiley, 2007). He holds several patents related to areas of dielectric resonator filters, superconductivity and MEMS devices. His current research interests include MEMS technology and miniature tunable RF filters for wireless and satellite applications.

Dr. Mansour is a Fellow of the Engineering Institute of Canada (EIC) and a Fellow of the Canadian Academy of Engineering (CAE).